Desalination and Water Treatment
www.deswater.com
doi: 10.5004/dwt.2021.27818

239 (2021) 259–269
November

La_2O_3 nanoparticles: synthesis and application for removal of arsenite and phosphate from water

Nguyen Quang Bac[a,b,*], Dao Ngoc Nhiem[a,b,*], Duong Thi Lim[c], Pham Ngoc Chuc[a], Doan Trung Dung[a], Nguyen Thi Ha Chi[a], Dao Hong Duc[b], Luu Thi Viet Ha[d], Dinh Quang Khieu[e]

[a]*Institute of Material Science, VAST, 10000, Vietnam, emails: quangbac1993@gmail.com (N. Quang Bac), nhiemdn@ims.vast.ac.vn (D. Ngoc Nhiem), chucpn@ims.vast.ac.vn (P. Ngoc Chuc), dungdt@ims.vast.ac.vn (D. Trung Dung), 2211hachi@gmail.com (N. Thi Ha Chi)*
[b]*Graduate University of Science and Technology, VAST, 10000, Vietnam, email: hongducmt@gmail.com (D. Hong Duc)*
[c]*Institute of Geography, VAST, 10000, Vietnam, email: duonglim79@gmail.com (D. Thi Lim)*
[d]*Faculty of Chemical Engineering, Industrial University of Ho Chi Minh City, 70000, Vietnam, email: thiviethaluu@gmail.com (L. Thi Viet Ha)*
[e]*University of Sciences, Hue University, 49000, Vietnam, email: dqkhieu@hueuni.edu.vn (D. Quang Khieu)*

Received 26 July 2021; Accepted 17 September 2021

ABSTRACT

In this study, La_2O_3 nanoparticles were manufactured utilizing a sol–gel combustion process with gelatin as a template, and they were used to remove phosphate and arsenite. X-ray diffraction, thermal analysis, energy-dispersive X-ray elemental mapping, transmission electron microscopy, and high-resolution transmission electron microscopy were used to characterize the materials. The morphology of La_2O_3 was discovered to be extensively scattered, with nanoparticles measuring 10–20 nm. In aqueous solutions, the produced La_2O_3 nanoparticles show good phosphate or arsenite adsorption capacity. The pseudo-second-order kinetic model is used to explain the adsorption of arsenite and phosphate on La_2O_3. Based on the Langmuir isotherm model, the phosphorus and arsenite adsorption capacities were 289.9 and 89.1 mg g^{-1}, respectively, the highest among those reported. Interestingly, the uptake of arsenite and phosphate followed a similar pattern which peaked at pH 7.1 at 25°C. Even after eighth cycles, the La_2O_3 nanoparticles show good adsorption with just a minor decrease of adsorption capacity (9.0% and 9.5% for arsenite and phosphate, respectively), showing that La_2O_3 is a promising material for aquatic treatment.

Keywords: La_2O_3 nanoparticles; Adsorption; Arsenite removal; Phosphate adsorption

1. Introduction

In natural waterways, phosphorus is a major problem for a number of biological and chemical processes. Excessive phosphorus emission into aquatic environments may cause eutrophication and thereby damage water quality. Phosphorus enters water sources through weathering of rocks and human activities such as the overuse of chemical fertilizers and the discharge of effluent from animal husbandry. The demand for phosphorus removal is growing as phosphorus-polluted water becomes more prevalent [1]. Arsenic is a very hazardous element that may be found in many parts of the world, particularly in Southeast Asia [2]. Natural processes, such as weathering of arsenic-containing

* Corresponding authors.

minerals and human actions, such as mining and the use of arsenical pesticides, both lead to increasing arsenic concentrations in aquatic ecosystems [3]. Long-term exposure to arsenic-contaminated water can result in health problems such as kidney, lung, liver, and prostate cancers, as well as skin lesions (such as skin pigmentation and the formation of hard patches of skin on the palms of the hands) [4]. Arsenic is found in nature mostly as arsenate (As(V)) and arsenite (As(III)). In comparison to As(V) species, As(III) is more poisonous, mobile, and difficult to immobilize [5,6]. As a result, many scientists are interested in the remediation of pollutants in water, such as arsenic or phosphate. Co-precipitation, adsorption, and ion exchange are some of the ways utilized to treat them [1,7,8]. Because of its effectiveness, low cost, low energy consumption, and ease of operation, the adsorption method is widely regarded as the best available [9,10]. The most crucial aspect of the adsorption process is to identify a good adsorbent that offers a variety of benefits while also matching the treatment requirements.

Metal oxide/hydroxide nanomaterials, such as iron, zirconium, titanium, manganese, and aluminum [10,11], have recently been widely used for removing arsenic or phosphate from polluted water because of their rich valence states, variable electronic structures, natural abundance, and stability in water solutions [12]. Rare-earth metal oxides have found widespread use in catalysts, fuel cells, and gas sensors [13,14], and among them, La_2O_3 is highly active as an adsorbent. Various approaches have been used to manufacture La_2O_3 and its La_2O_3-based materials with the goal of enhancing the adsorption capacity and durability for practical usage. Long et al. [15] reported the combustion synthesis of nanocrystalline La_2O_3 using an ethanol amine-nitrate method, and the nanocrystalline La_2O_3 has good dye adsorption properties. The effective adsorption of phosphate and arsenic species is demonstrated by La_2O_3 supported porous materials such as MCM-41, zeolite, and activated carbons [16–18]. Despite the fact that La_2O_3 has a high adsorption capacity to anions such as arsenite or phosphate, few articles on arsenic and phosphate adsorption of La_2O_3 have been published to our knowledge.

The application of combustion synthesis of nanoparticles La_2O_3 utilizing a gelatin template to remove phosphate and arsenate from aqueous solutions is described in the current paper. The phosphate and arsenate adsorption properties of the derived La_2O_3 are exceptional. Effects of pH, temperature and competing ions on the adsorption of La_2O_3 nanoparticles were investigated. Besides, the kinetics of adsorption and the mechanism of adsorption have been studied thoroughly.

2. Experimental

2.1. Materials

Gelatin (M_w = 834, $C_{35}H_{54}N_{12}O_{12}$), lanthanum(III) nitrate hexahydrate ($La(NO_3)_3{\cdot}6H_2O$, 99%), sodium (meta) arsenite ($NaAsO_2$, 99%), and potassium dihydrogen phosphate (KH_2PO_4, 99%) are purchased from Merck (USA) without any further modification.

Sodium arsenite was dissolved in distilled water to make the arsenite (As(III)) stock solution. The arsenite solutions are made daily by diluting the stock solution accordingly. Arsenic species concentrations are always expressed in terms of elemental arsenic concentrations.

Phosphate stock solutions were made by dissolving an exact amount of anhydrous potassium phosphate in distilled water to a concentration of 1,000 mg L^{-1}, then diluting with distilled water as needed. Phosphorus content is expressed as phosphate concentration.

2.2. Synthesis of La_2O_3

A magnetic stirrer was used to agitate the gelatin (0.834 g) and distilled water (50 mL) until the gelatin was completely dissolved. The gelatin solution was then added to 5 mL of 0.01 M lanthanum nitrate solution, then adjusted to the required pH with dilute HCl or KOH solution. The mixture was further agitated until a gel was formed. Finally, the gel was dried for 24 h at 110°C before being calcined for 2 h at 180°C, 450°C, 550°C, and 650°C to obtain La_2O_3 nanoparticles.

2.3. Apparatus

X-ray diffraction (XRD) was performed on a D8 ADVANCE Bruker (Germany) with CuKα = 0.15406 nm. Thermal analysis (TG-DTA) was recorded in the ambient atmosphere from room temperature to 850°C using SETARAM (France). Energy-dispersive X-ray elemental mapping was conducted on a D8 ADVANCE Bruker (Germany). Transmission electron microscopy (TEM) and high-resolution transmission electron microscopy were studied with S4800-NIHE (Japan). The arsenic element was measured by atomic absorption spectroscopy (AAS) using a Perkin Elmer AAnalyst 200 (USA) with acetylene flame (F-AAS) and a wavelength of 193.7 nm. The phosphate concentration was determined with the spectrophotometric method using vanadate-molybdate reagent according to Vietnam's standard (TCVN 6202:2008).

2.4. Adsorption experiments

2.4.1. Point of zero charges (pH_{PZC})

The pH drift method was used to determine the pH_{PZC}. As an inert electrolyte, 0.1 g of La_2O_3 was added to 50 mL of 0.1 M NaCl solution. Using 0.01 M NaOH or 0.01 M HCl solutions, the starting pH ($pH_{initial}$) was adjusted from 2 to 12. To establish adsorption/desorption equilibrium, the suspension was agitated for 24 h at room temperature using a shaker. Following that, the supernatant was collected, and the pH was reported (pH_{final}). The difference between $pH_{initial}$ and pH_{final} vs. $pH_{initial}$ was plotted, and the value of pH_{PZC} was determined by the point of intersection of the curve with the abscissa.

A similar approach was used to test the altering pH_{PZC} in phosphate or arsenite adsorption, in which 50 mL of the inert electrolyte solution was supplemented with 0.3 mg of NaH_2PO_4 or 0.1 mg of Na_2AsO_2.

2.4.2. Kinetics and thermodynamic studies

The kinetics of adsorption was studied in batches. The adsorption process was carried out in a 2-liter beaker

with a mechanical stirrer. At room temperature, 0.125 g of La_2O_3 was added to 250 mL of arsenite or phosphate solution in the beaker. A centrifuge was used to separate the filtrate from 3 mL of the solution drawn at a specific time.

The detailed calculation is presented as in the supplementary document [Eqs. (1)–(4)].

2.4.3. Equilibrium adsorption

0.05 g La_2O_3 was added to eight 200 mL flasks containing 100 mL of various adsorbate concentrations (i.e., 1, 5, 10, 20, 50, 100, 150, 200, and 250 mg L^{-1} for arsenite and 5, 10, 20, 40, 60, 80, 100, 150, 200, and 250 mg L^{-1} for phosphate). A shaker was used to stir the flasks for 24 h at room temperature. After that, the supernatant was centrifuged, and the adsorbate concentration was determined.

The detailed calculation is presented as in the supplementary document [Eqs. (5)–(10)].

2.4.4. Desorption of adsorbents

The saturated NaCl solution was used to recycle the used La_2O_3 nanoparticles. Pass the saturated NaCl solution through a column containing the used La_2O_3 nanoparticles several times to remove the adsorbates (arsenite or phosphate) completely. Before reuse, the rejuvenated La_2O_3 nanoparticles were taken from the column, washed in acid and basic solutions, and dried at 100°C for 24 h.

All the above experiments were repeated at least three times to observe the repeatability of the result. The standard deviation in this study was relatively small, which indicated that no significant deviations were observed.

3. Results and discussion

3.1. Characterization of prepared materials

Thermogravimetry-differential scanning calorimetry (TG-DSC) was used to investigate the thermal behavior of $La(NO_3)_3$/gelatin precursor. The result is shown in Fig. 1.

On the TGA curve, three mass losses were shown. The first, which corresponded to a 15.39% mass loss and an exothermic effect that peaked at 225°C, may be attributed to gelatin combustion with low molecular weights. The breakdown of gel sample $La(NO_3)_3$/gelatin and nitrate salts was assigned to the second one, which has a sample weight loss of 15.9% in the temperature range 226°C–400°C and an exothermic effect that peaked at 321°C. Finally, the most substantial weight loss, around 23.43% in the temperature range of 330°C–500°C, corresponding to the exothermic impact that peaked at 465°C, was most likely attributable to gelatin's burning reaction in the gel. This temperature range initiates the formation of the La_2O_3 phase.

XRD was used to investigate the influence of calcination temperature on the development of the La_2O_3 phase. Fig. 2 indicates the XRD patterns of prepared material at some calcination temperature.

The figure shows that the $La(NO_3)_3$-gelatin precursor does not exhibit any typical peaks of the La_2O_3 phase when heated to 180°C. The features of the La_2O_3 phase occur when the temperature is raised to 450°C, although it was not obvious (JCPDS: No 01-083-1344). The distinct and strong diffraction peaks of the La_2O_3 phase were produced when heating temperatures approached 550°C and 650°C. As a result, the sample calcination temperature of 550°C was chosen for subsequent studies to synthesis La_2O_3.

XRD analysis was also utilized to investigate the pH influence on the development of the La_2O_3 phase. The results are shown in Fig. 3.

It was discovered that pH had no effect on the development of the La_2O_3 phase when pH values varied from 2 to 5. This is owing to the fact that the complex of La^{3+} is stable in gelatin solution. Following research, pH 5 was chosen for material preparation. Fig. 3b depicts the XRD patterns of La_2O_3 produced at various gel-forming temperatures. This suggests that, under experimental conditions, the gel-forming temperature has minimal influence on La_2O_3 phase development. Temperature, on the other hand, has a major impact on the time necessary for gel formation. La(III) ion transport into the gelatin network was low at 40°C and 60°C. Due to the poor diffusion of La(III) ions into the gelatin network at a low temperature of 40°C–60°C, the gel formation process takes a long time (7–8 h). However, the higher temperature of gel formation at 80°C, 100°C times was lowered in half to 2–3 h. As a result, the gel formation temperature of 80°C was chosen to assist the future study experiments.

Scanning electron microscopy (SEM) and TEM were used to examine the morphology of La_2O_3 (Fig. 4). SEM inspection

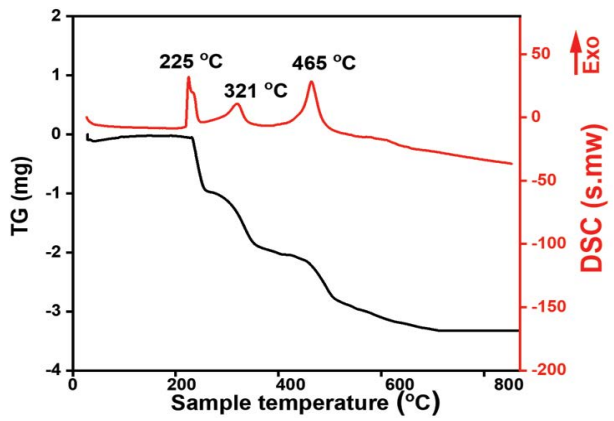

Fig. 1. TG-DSC diagrams of $La(NO_3)_3$/gelatin gel.

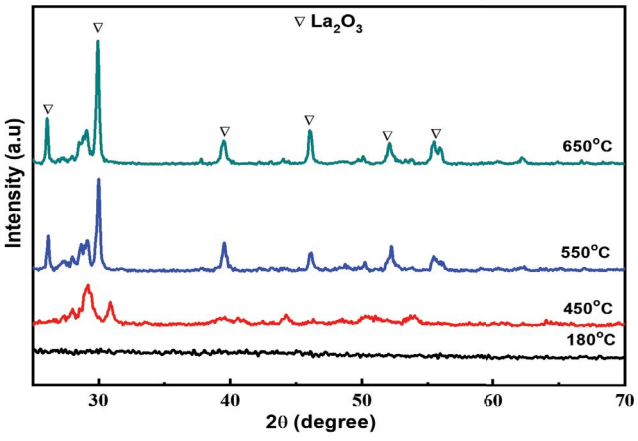

Fig. 2. XRD patterns at different calcination temperatures.

reveals a significant aggregation at 500–1,000 nm (Fig. 4a). These particles, as shown in the TEM picture, have a spherical shape and a uniform size of 10 nm (Fig. 4b).

The nitrogen adsorption/desorption isotherms are used to investigate the textural properties of La_2O_3 (Fig. 5). According to the IUPAC classification, the isotherm curve is of type III. The BET model calculated a specific surface area of 37.8 $m^2\ g^{-1}$.

3.2. *Phosphate and arsenite adsorption of La_2O_3 nanomaterial*

Fig. 6 shows the influence of pH on phosphate and arsenite adsorption. The reaction temperature was kept constantly at 25°C.

Phosphate uptake increases with pH from 2 to 7, peaks at approximately pH 7.1, and decreases with higher pH (Fig. 6a). The uptake of arsenite follows a similar pattern (Fig. 6b). At pH 7.1, phosphate adsorption was approximately 77.72 mg g^{-1}, and arsenite uptake was approximately 1.98 mg g^{-1}.

Phosphate has three pKa values (pK_1 = 2.20, pK_2 = 7.2, and pK_3 = 12.3) [19], but arsenite is likewise a polyprotic acid with pK_1 = 9.23, pK_2 = 12.1, and pK_3 = 13.41. The pH of the solution at the point of zero charge (pH_{PZC}) was 7.2. (Fig. 7). As a result, at pH > 7.2, the anionic species of arsenite ($H_2AsO_3^-$, $HAsO_3^{2-}$) or phosphate ($H_2PO_4^-$, HPO_4^{2-}, and PO_4^{3-}) have the same charge as the La_2O_3 surface, producing

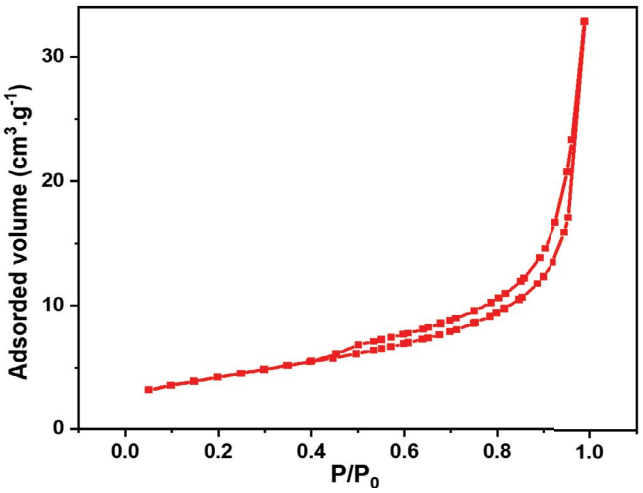

Fig. 5. Nitrogen adsorption/desorption isotherms of La_2O_3.

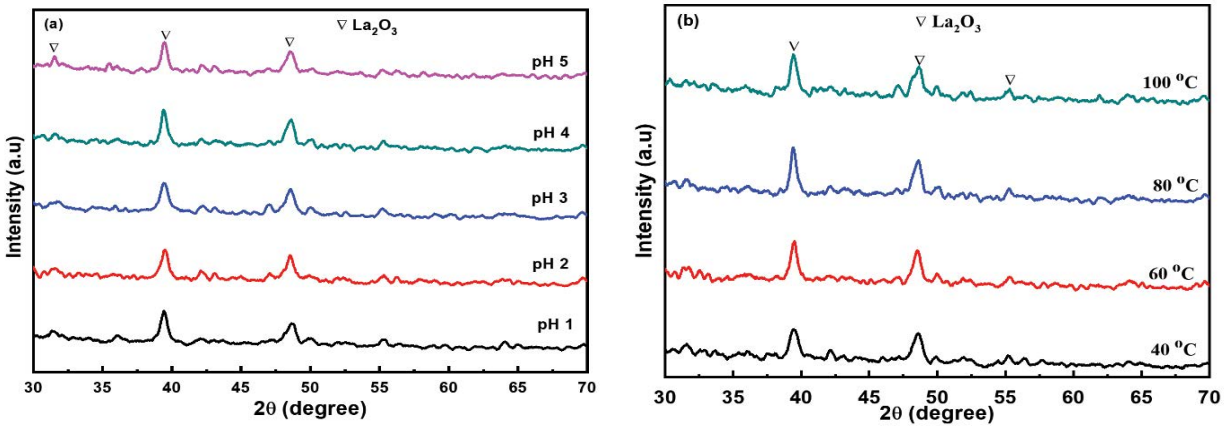

Fig. 3. Effect of (a) pH and (b) temperature of gel formation.

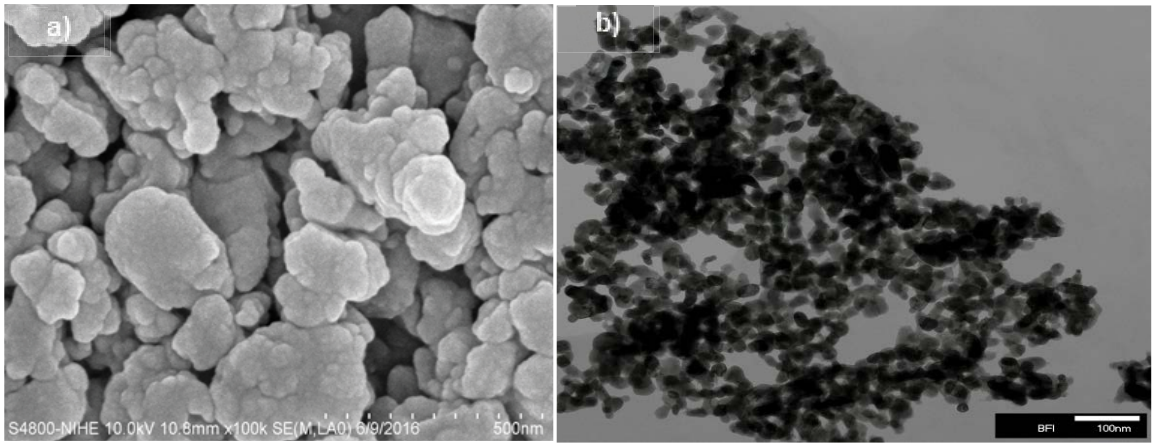

Fig. 4. (a) SEM and (b) TEM images of La_2O_3 nanoparticles.

electrostatic repulsion between the adsorbate and the adsorbent resulting in low arsenite or phosphate adsorbability.

The pH_{PZC} fell from 7.2 (in inert electrolyte solution) to 6.1 (in 1 mg L^{-1} $NaAsO_2$) and 6.7 (in 6 mg L^{-1} PO_4^{3-}) in the presence of adsorbed phosphate or arsenite (Fig. 7). This pH_{PZC} change also indicates a form of selective adsorption rather than merely physical adsorption. The development of outer-sphere surface complexes could not shift the pH_{PZC} of metal oxides because the adsorbent could not modify the surface owing to no specific chemical interactions between the adsorbate and the adsorbent [20]. In the current work, the pH_{PZC} shift indicates the development of anion–negatively charged surface complexes. As a result, the reduction in pH_{PZC} might be caused by negatively charged inner-sphere complexes formed by phosphate or As(III) with the adsorbent [1,21].

The presence of the La-OH functional group promotes adsorption, which favors the ligand exchange process [22], and phosphates replace the hydroxyl groups at the active sites through inner-sphere complexes [1,19,23], as shown in Fig. 8. At pH 9, arsenite functions as a weak acid, and the neutral species ($HAsO_2$) prevail. As illustrated in Fig. 8, the neutral As(III) ($HAsO_2$) can adsorb on the La-OH functional group via the formation of monodentate complexes, as predicted by Li et al. [24].

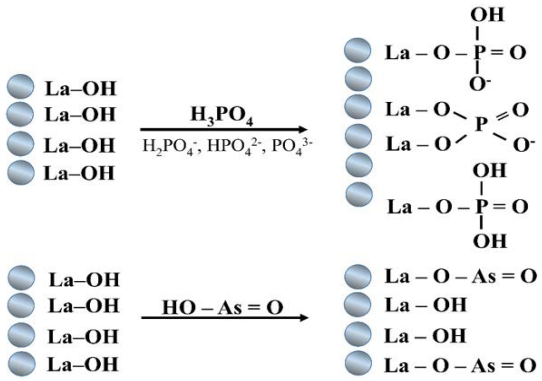

Fig. 8. The schematic diagram for phosphate adsorption (upper) and arsenite adsorption (lower) on La_2O_3.

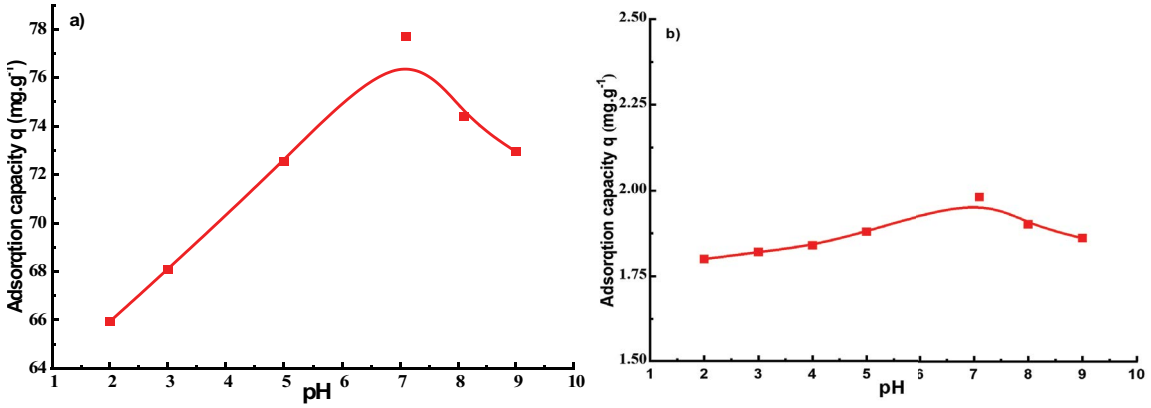

Fig. 6. The pH effect on (a) phosphate and (b) arsenite adsorption using La_2O_3 (mass: 0.05 g; initial conc.: 100 mg L^{-1}; contact time: 240 min; temperature: 25°C)

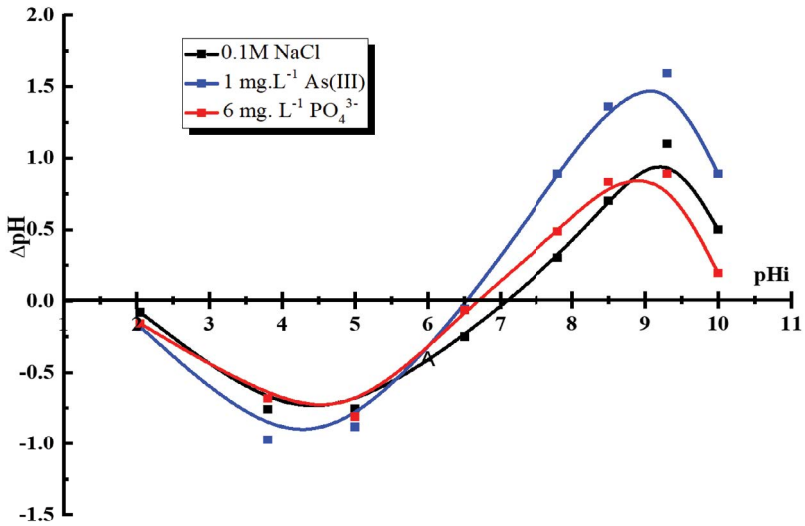

Fig. 7. pH_{PZC} of La_2O_3 in the inert electrolyte and the presence of arsenite and phosphate.

3.2.1. Adsorption kinetics

The adsorption of phosphate or arsenite were affected by both the contact duration with the adsorbent and the initial adsorbate concentrations. Fig. 9 depicts the time dependence of adsorbent adsorption at the two starting adsorbate concentrations. As seen in the figure, phosphate adsorption rises as contact duration increases until equilibrium is reached. After 100 min, the equilibrium is reached. Arsenite adsorption followed a similar pattern. The only difference was that the equilibrium time was shorter, about 80 min. The pseudo-second-order rate model is used for both kinetic data (Tables 1 and 2). According to the pseudo-second-order kinetic model, chemosorption [25,26] occurs between phosphate or arsenite and the La_2O_3 oxide, involving valent forces through electron sharing or exchange between the adsorbent and the adsorbate by replacing –OH with phosphate and arsenite, as shown in Fig. 8.

3.2.2. Thermodynamic parameters

The phosphate and arsenite uptake on La_2O_3 was increased with an increase in temperature. The adsorption uptake increases from 73.82 mg g^{-1} at 293 K to 75.98 mg g^{-1} at 313 K for phosphate and 14.1 mg g^{-1} at 293 K to 14.84 mg g^{-1} for arsenite, indicating that phosphate and arsenite adsorption is endothermic in nature in the studied temperature range, which is a chemosorption, as mentioned above.

The thermodynamic parameters are determined via a linear plot of the logarithm of the rate constant and the reciprocal temperature (Fig. 10). The slope and intercept of this linear plot were used to compute $\Delta H°$ (20.11 kJ mol^{-1} for phosphate adsorption and 44.77 kJ mol^{-1} for arsenite adsorption) and $\Delta S°$ (0.81 kJ mol^{-1} for phosphate adsorption and 0.23 kJ mol^{-1} for arsenite adsorption). Positive $\Delta H°$ levels in nature indicate an endothermic reaction. Positive $\Delta S°$ values suggest that phosphate or arsenite anions have a strong affinity for the adsorbent and that unpredictability at the solid-solution interface increases during adsorption [27]. The presence of negative $\Delta G°$ values indicates that the adsorption of arsenite or phosphate onto La_2O_3 is thermodynamically spontaneous. There is unnecessary to take external energy for this adsorption process [28,29]. With increasing temperature, $\Delta G°$ decreases from –2.15 to –2.86 kJ mol^{-1} for phosphate adsorption and from –0.31 to

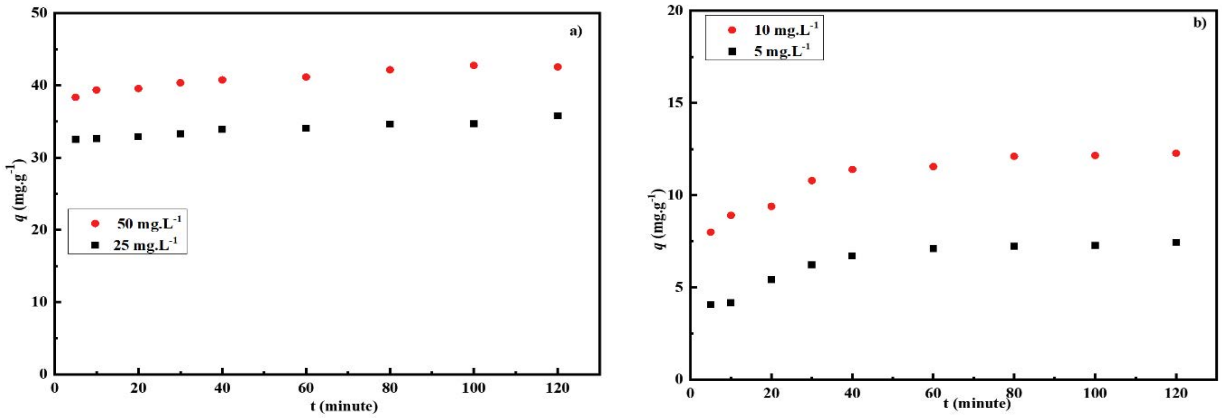

Fig. 9. Kinetics of (a) phosphate adsorption and (b) at arsenite adsorption different initial phosphate concentration on La_2O_3 (La_2O_3 weight: 0.05 g; initial phosphate: 25 and 50 mg L^{-1} (250 mL); initial arsenite concentration: 5 and 10 mg L^{-1} (250 mL)).

Table 1
The parameters of pseudo-kinetics for phosphate adsorption on to La_2O_3

Conc. (mg L^{-1})	Pseudo-first-order kinetic equation				Pseudo-second-order kinetic equation		
	q_e (mg g^{-1})	q_{1model} (mg g^{-1})	k_1 (min^{-1})	R^2	q_{2model} (mg g^{-1})	k_2 (g mg^{-1} min^{-1})	R^2
25	37.82	5.610	0.007	0.9346	38.17	0.0057	0.997
50	75.56	5.278	0.016	0.9456	75.75	0.0100	0.999

Table 2
The parameters of formal kinetics for arsenite adsorption on to La_2O_3

Conc. (mg L^{-1})	Pseudo-first-order kinetic equation				Pseudo-second-order kinetic equation		
	q_e (mg g^{-1})	q_{1model} (mg g^{-1})	k_1 (min^{-1})	R^2	q_{2model} (mg g^{-1})	k_2 (g mg^{-1} min^{-1})	R^2
5	7.76	3.45	0.0276	0.977	7.867	0.0173	0.998
10	14.82	5.37	0.0414	0.962	15.222	0.0170	0.994

–0.55 kJ mol^{-1} for arsenate adsorption (Table 3), implying that more phosphate or arsenite species are adsorbed.

3.2.3. Equilibrium adsorption

The non-linear Langmuir and Freundlich models were used to fit the isothermal data of phosphate and arsenite adsorption onto La_2O_3 nanoparticles (Fig. 11). The equilibrium adsorption data fit better with the Langmuir isotherm model due to its high R^2 values of 0.97 for phosphate and 0.96 when compared to the Freundlich model, which was 0.92 and 0.85, respectively (Table 4). The Langmuir adsorption capacity (q_m) of phosphate is around 289.9 and 89.10 mg g^{-1} for arsenite, both of which are among the highest values documented in the literature (Table 5). The recent findings suggest that La_2O_3 might be used to treat arsenic or phosphate-polluted wastewaters.

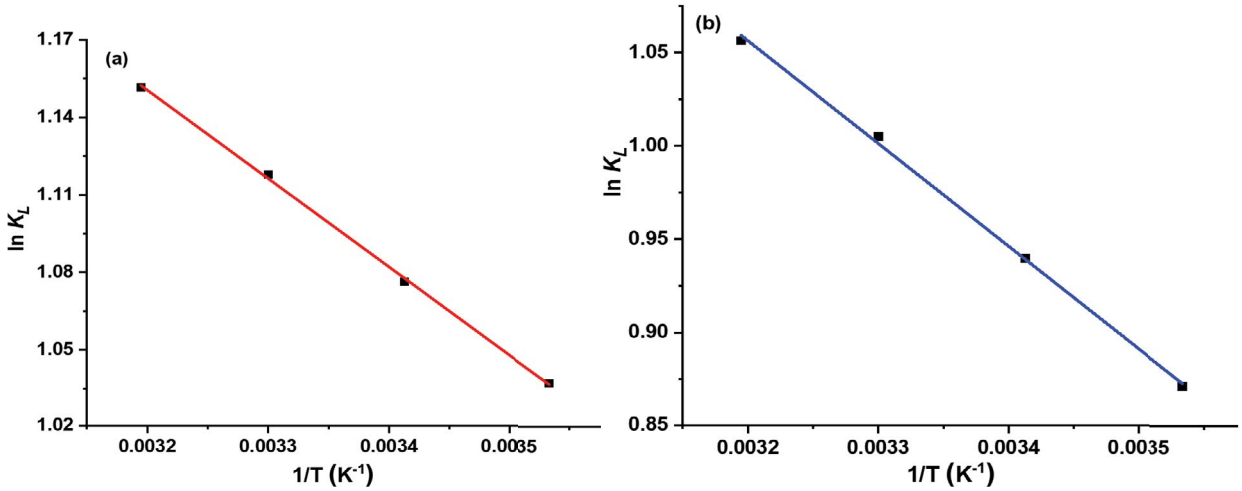

Fig. 10. The Arrhenius plot of ln$K$ and 1/T for (a) phosphate and (b) arsenite adsorption.

Table 3
The parameters of thermodynamics for phosphate and arsenite adsorption

	Arsenite adsorption			Phosphate adsorption		
T (K)	$\Delta H°$ (kJ mol^{-1})	$\Delta S°$ (kJ mol^{-1} K^{-1})	$\Delta G°$ (kJ mol^{-1})	$\Delta H°$ (kJ mol^{-1})	$\Delta S°$ (kJ mol^{-1} K^{-1})	$\Delta G°$ (kJ mol^{-1})
283	44.77	0.23	–2.15	20.11	0.81	–0.31
293			–2.39			–0.39
303			–2.62			–0.47
313			–2.86			–0.55

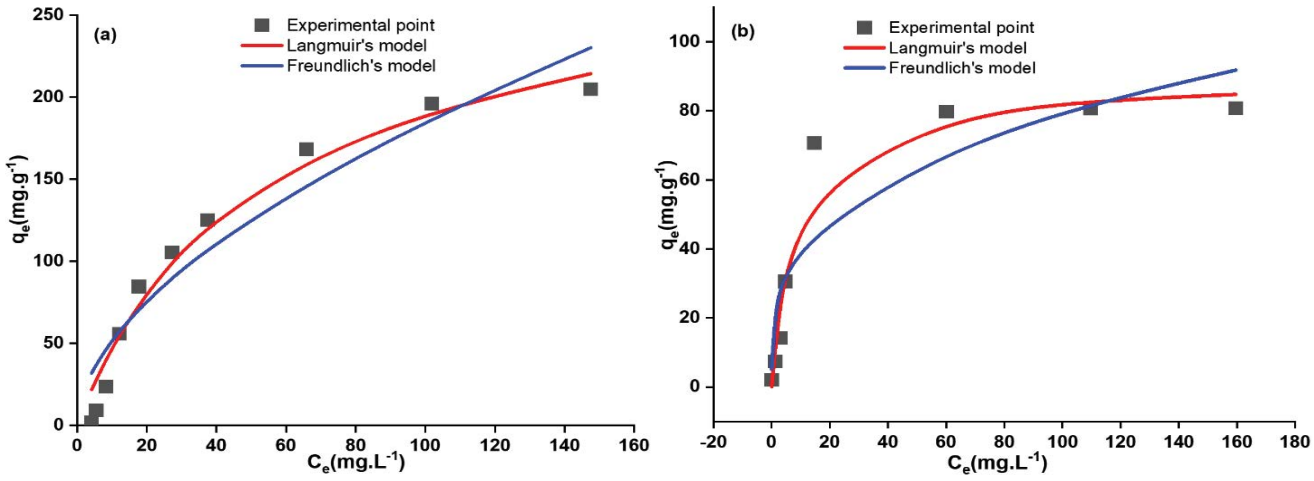

Fig. 11. Adsorption equilibrium isotherms of (a) phosphate and (b) arsenite on La_2O_3.

3.2.4. Competing ions

The effect of competing ions such as Fe(III), Mn(II), Cl^-, and SO_4^{2-} on phosphate or arsenite adsorption by the acquired La_2O_3 nanoparticles was investigated. Table 6 shows the outcomes of the competing ions.

The arsenite adsorption capacity raised from 7.36 to 9.98 mg g^{-1} when the Fe(III) concentration increased 1.78 times. This might be attributed to the combination of Fe(III) and arsenite on the material's surface, which increases adsorption. When Mn(II) concentrations increased 1.85 times, arsenite removal dropped by 13%. A similar cation impact on La_2O_3 phosphate adsorption was found, with the addition of Fe(III) and Mn(II) increasing its adsorption capability. The effect of sulfate or chloride on phosphate and arsenite adsorption was minimal. For example, when the chloride concentration was 14.08 times that of arsenite, the adsorption capacity of phosphate only fell by 7.6%. Notably, the amounts of competing anions in this research were significantly greater than those found in groundwater. Thus, even at extremely high concentrations of the competing anions utilized in this work, La_2O_3 nanoparticles can adsorb arsenite and phosphate effectively.

3.2.5. Regenerability

La_2O_3 nanomaterials could be efficiently regenerated so that they may be utilized for numerous operations cycles. In the fixed column bed, the used adsorbent was regenerated with the saturation solution. Slowly, the prepared solution went through the fixed bed. The first cycle recovered more than 70% of the adsorbed phosphate or arsenite, while successive cycles recovered almost 100% of the adsorbed phosphate or arsenite. The adsorption capacity of recycled La_2O_3 nanoparticles was never less than 90% of the initial La_2O_3 nanoparticles in the eight regeneration tests (Fig. 12a). Fig. 12b depicts a comparison of XRD patterns of 8th reused La_2O_3 nanoparticles to those of fresh La_2O_3. The very small decrease in the strength of distinctive peaks after the eighth recycling indicates that the La_2O_3 nanoparticles were recyclable (Fig. 12b).

Table 4
The parameters of Langmuir and Freundlich isotherm models at the room temperature

Models	Langmuir isotherm model			Freundlich isotherm model		
Parameters	q_m (mg g^{-1})	K_L	R^2	K_F	n	R^2
Phosphate adsorption	289.90	0.02	0.97	14.31	1.80	0.92
Arsenite adsorption	89.10	0.12	0.96	20.27	3.35	0.85

Table 6
Effect of some ions on to phosphate and arsenic adsorption of La_2O_3 nanomaterial

Interfering ions	Molar ratio[a]	q_e (mg g^{-1})[b]	Molar ratio[a]	q_e (mg g^{-1})[b]
Fe(III)	0	72.48	0	7.36
	0.17	74.66	0.8	7.94
	0.25	75.14	1.25	9.54
	0.35	77.78	1.78	9.98
Mn(II)	0	72.48	0	7.36
	0.18	73.92	0.92	7.92
	0.25	74.06	1.29	8.66
	0.37	76.02	1.85	9.58
Cl^-	0	72.48	0	7.36
	2.81	68.36	14.08	6.36
	5.63	66.96	28.16	5.96
	14.08	62.64	70.42	5.64
SO_4^{2-}	0	72.48	0	7.36
	1.04	72.08	5.20	7.08
	2.08	71.84	10.41	6.7
	5.20	71.76	26.04	6.06

[a]interferent/adsorbate molar ratio;
q_e: the adsorption capacity.

Table 5
Comparison of adsorption performance of the present adsorbents with previous works

Adsorbents	Phosphate		Adsorbents	Arsenite	
	q_m (mg g^{-1})	Ref.		q_m (mg g^{-1})	Ref.
Modified bentonites	11.15	[30]	Degussa P25	3.9	[31]
Iron hydroxide-eggshell waste	10.6	[32]	TiO_2 suspensions	42.1	[31]
Al-bentonite	12.7	[22]			
Iron-doped activated carbon	14.2	[33]	Natural laterite	0.58	[34]
La(III)/modified zeolite	24.6	[17]	Fe_3O_4 nanoparticles (diameter: 12 nm)	133.37	[35]
Fe-Al-Mn trimetal oxide	48.3	[36]	Fe/OMC	8.2	[37]
Tantalum hydroxide	78.5–97.0	[38]	CuO nanoparticles	26.90	[39]
ZrO_2 amorphous nanoparticles	99.01	[26]	$MnFe_2O_4$	93.8	[20]
La_2O_3	289.9	Present work	La_2O_3	89.10	Present work

OMC: Ordered mesoporous carbon

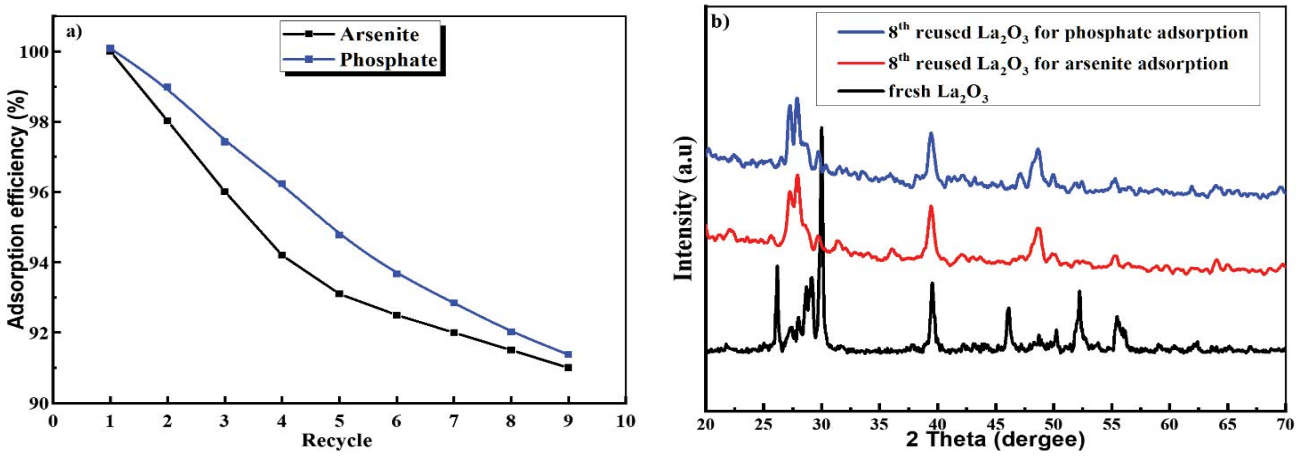

Fig. 12. (a) Adsorption capacity after reuse and (b) XRD patterns of the fresh and the 8th reused La_2O_3.

4. Conclusions

The La_2O_3 nanoparticles were synthesized utilizing the sol–gel combustion technique with gelatin as a template. The resulting La_2O_3 nanoparticles display significant phosphate and arsenite adsorption. La_2O_3 nanoparticles have a high phosphate and arsenic adsorption capacity of 289.90 and 89.10 mg g^{-1}, respectively. After the ninth recycling, the current La_2O_3 nanoparticles remain stable with a slight decrease in adsorption activity. These findings demonstrate that the La_2O_3 nanomaterials are an efficient adsorbent for phosphate or arsenite removal.

Data availability

The data used to support the findings of this study are available from the corresponding author upon request.

Conflicts of interest

The authors declare that they have no conflicts of interest.

Acknowledgments

This study is funded by the Vietnam National Foundation for Science and Technology Development (NAFOSTED) under grant number: NCUD-01-2019.58.

Symbols

q_{1model}	—	Equilibrium adsorption capacity following the pseudo-first-order kinetic model, mg g^{-1}
k_1	—	Rate constant for the pseudo-first-order kinetic model, min^{-1}
R^2	—	Regression coefficient
q_{2model}	—	Equilibrium adsorption capacity following the pseudo-second-order kinetic model, mg g^{-1}
k_2	—	Rate constant for the pseudo-second-order kinetic model, g mg^{-1} min^{-1}
K_L	—	Langmuir equilibrium constant, L mg^{-1}
$\Delta H°$	—	Standard enthalpy, kJ mol^{-1}
$\Delta S°$	—	Standard entropy, kJ mol^{-1} K^{-1}
$\Delta G°$	—	Standard Gibbs free energy, kJ mol^{-1}
K_F	—	Freundlich equilibrium constant
T	—	Kelvin temperature, K
K_d	—	Distribution coefficient
q_m	—	Maximum adsorption capacity of the monolayer, mg g^{-1}
q_e	—	Equilibrium adsorption capacity, mg g^{-1}
C_e	—	Dye concentration at equilibrium, mg L^{-1}

References

[1] R. Chitrakar, S. Tezuka, A. Sonoda, K. Sakane, K. Ooi, T. Hirotsu, Phosphate adsorption on synthetic goethite and akaganeite, J. Colloid Interface Sci., 298 (2006) 602–608.
[2] L.H.E. Winkel, P.T.K. Trang, V.M. Lan, C. Stengel, M. Amini, N.T. Ha, P.H. Viet, M. Berg, Arsenic pollution of groundwater in Vietnam exacerbated by deep aquifer exploitation for more than a century, Proc. Natl. Acad. Sci. U.S.A., 108 (2011) 1246–1251.
[3] S. Kleinert, E.M. Muehe, N.R. Posth, U. Dippon, B. Daus, A. Kappler, Biogenic Fe(III) minerals lower the efficiency of iron-mineral-based commercial filter systems for arsenic removal, Environ. Sci. Technol., 45 (2011) 7533–7541.
[4] M.R. Awual, M.A. Shenashen, T. Yaita, H. Shiwaku, A. Jyo, Efficient arsenic(V) removal from water by ligand exchange fibrous adsorbent, Water Res., 46 (2012) 5541–5550.
[5] S.L. Shumlas, S. Singireddy, A.C. Thenuwara, N.H. Attanayake, R.J. Reeder, D.R. Strongin, Oxidation of arsenite to arsenate on birnessite in the presence of light, Geochem. Trans., 17 (2016), doi: 10.1186/s12932-016-0037-5.
[6] J.S. Yamani, S.M. Miller, M.L. Spaulding, J.B. Zimmerman, Enhanced arsenic removal using mixed metal oxide impregnated chitosan beads, Water Res., 46 (2012) 4427–4434.
[7] M. Pirilä, M. Martikainen, K. Ainassaari, T. Kuokkanen, R.L. Keiski, Removal of aqueous As(III) and As(V) by hydrous titanium dioxide, J. Colloid Interface Sci., 353 (2011) 257–262.
[8] M. Leist, R.J. Casey, D. Caridi, The management of arsenic wastes: problems and prospects, J. Hazard. Mater., 76 (2000) 125–138.
[9] Z. Wu, W. Li, P.A. Webley, D. Zhao, General and controllable synthesis of novel mesoporous magnetic iron oxide@carbon encapsulates for efficient arsenic removal, Adv. Mater., 24 (2012) 485–491.
[10] J. Mertens, J. Rose, R. Kägi, P. Chaurand, M. Plötze, B. Wehrli, G. Furrer, Adsorption of arsenic on polyaluminum granulate, Environ. Sci. Technol., 46 (2012) 7310–7317.

[11] L.C.A. Oliveira, D.I. Petkowicz, A. Smaniotto, S.B.C. Pergher, Magnetic zeolites: a new adsorbent for removal of metallic contaminants from water, Water Res., 38 (2004) 3699–3704.
[12] B. Wang, H. Wu, L. Yu, R. Xu, T.T. Lim, X.W. Lou, Template-free formation of uniform urchin-like α-FeOOH hollow spheres with superior capability for water treatment, Adv. Mater., 24 (2012) 1111–1116.
[13] C.T. Campbell, C.H.F. Peden, Oxygen vacancies and catalysis on ceria surfaces, Science, 309 (2005) 713–714.
[14] Q. Yuan, H.H. Duan, L.L. Li, L.D. Sun, Y.W. Zhang, C.H. Yan, Controlled synthesis and assembly of ceria-based nanomaterials, J. Colloid Interface Sci., 335 (2009) 151–167.
[15] Y. Long, J. Yang, X. Li, W. Huang, Y. Tang, Y. Zhang, Combustion synthesis and stability of nanocrystalline La_2O_3 via ethanolamine-nitrate process, J. Rare Earths, 30 (2012) 48–52.
[16] X. Jia, X. He, K. Han, Y. Ba, X. Zhao, Q. Zhang, La_2O_3-modified MCM-41 for efficient phosphate removal synthesized using natural diatomite as precursor, Water Sci. Technol., 79 (2019) 1878–1886.
[17] P. Ning, H.J. Bart, B. Li, X. Lu, Y. Zhang, Phosphate removal from wastewater by model-La(III) zeolite adsorbents, J. Environ. Sci., 20 (2008) 670–674.
[18] S. Yan, Q. An, L. Xia, S. Liu, S. Song, J.R. Rangel-Méndez, As(V) removal from water using the La(III)-montmorillonite hydrogel beads, React. Funct. Polym., 147 (2020) 104456, doi: 10.1016/j.reactfunctpolym.2019.104456.
[19] Y. Arai, D.L. Sparks, ATR-FTIR spectroscopic investigation on phosphate adsorption mechanisms at the ferrihydrite-water interface, J. Colloid Interface Sci., 241 (2001) 317–326.
[20] S. Zhang, H. Niu, Y. Cai, X. Zhao, Y. Shi, Arsenite and arsenate adsorption on coprecipitated bimetal oxide magnetic nanomaterials: $MnFe_2O_4$ and $CoFe_2O_4$, Chem. Eng. J., 158 (2010) 599–607.
[21] M.E. Pena, G.P. Korfiatis, M. Patel, L. Lippincott, X. Meng, Adsorption of As(V) and As(III) by nanocrystalline titanium dioxide, Water Res., 39 (2005) 2327–2337.
[22] L.G. Yan, Y.Y. Xu, H.Q. Yu, X.D. Xin, Q. Wei, B. Du, Adsorption of phosphate from aqueous solution by hydroxy-aluminum, hydroxy-iron and hydroxy-iron-aluminum pillared bentonites, J. Hazard. Mater., 179 (2010) 244–250.
[23] J. Antelo, M. Avena, S. Fiol, R. López, F. Arce, Effects of pH and ionic strength on the adsorption of phosphate and arsenate at the goethite-water interface, J. Colloid Interface Sci., 285 (2005) 476–486.
[24] Z. Li, S. Deng, G. Yu, J. Huang, V.C. Lim, As(V) and As(III) removal from water by a Ce-Ti oxide adsorbent: behavior and mechanism, Chem. Eng. J., 161 (2010) 106–113.
[25] S. Azizian, Kinetic models of sorption: a theoretical analysis, J. Colloid Interface Sci., 276 (2004) 47–52.
[26] Y. Su, H. Cui, Q. Li, S. Gao, J.K. Shang, Strong adsorption of phosphate by amorphous zirconium oxide nanoparticles, Water Res., 47 (2013) 5018–5026.
[27] E.I. Unuabonah, K.O. Adebowale, B.I. Olu-Owolabi, Kinetic and thermodynamic studies of the adsorption of lead(II) ions onto phosphate-modified kaolinite clay, J. Hazard. Mater., 144 (2007) 386–395.
[28] S. Agarwal, N. Sadeghi, I. Tyagi, V.K. Gupta, A. Fakhri, Adsorption of toxic carbamate pesticide oxamyl from liquid phase by newly synthesized and characterized graphene quantum dots nanomaterials, J. Colloid Interface Sci., 478 (2016) 430–438.
[29] V.K. Gupta, A. Fakhri, S. Agarwal, A.K. Bharti, M. Naji, A.G. Tkachev, Preparation and characterization of TiO_2 nanofibers by hydrothermal method for removal of Benzodiazepines (Diazepam) from liquids as catalytic ozonation and adsorption processes, J. Mol. Liq., 249 (2018) 1033–1038.
[30] M. Zamparas, A. Gianni, P. Stathi, Y. Deligiannakis, I. Zacharias, Removal of phosphate from natural waters using innovative modified bentonites, Appl. Clay Sci., 62–63 (2012) 101–106.
[31] P.K. Dutta, A.K. Ray, V.K. Sharma, F.J. Millero, Adsorption of arsenate and arsenite on titanium dioxide suspensions, J. Colloid Interface Sci., 278 (2004) 270–275.
[32] N.Y. Mezenner, A. Bensmaili, Kinetics and thermodynamic study of phosphate adsorption on iron hydroxide-eggshell waste, Chem. Eng. J., 147 (2009) 87–96.
[33] Z. Wang, E. Nie, J. Li, M. Yang, Y. Zhao, X. Luo, Z. Zheng, Equilibrium and kinetics of adsorption of phosphate onto iron-doped activated carbon, Environ. Sci. Pollut. Res., 19 (2012) 2908–2917.
[34] M.K. Purkait, A. Maiti, S. DasGupta, S. De, Removal of congo red using activated carbon and its regeneration, J. Hazard. Mater., 145 (2007) 287–295.
[35] S. Yean, L. Cong, C.T. Yavuz, J.T. Mayo, W.W. Yu, A.T. Kan, V.L. Colvin, M.B. Tomson, Effect of magnetite particle size on adsorption and desorption of arsenite and arsenate, J. Mater. Res., 20 (2005) 3255–3264.
[36] J. Lǔ, H. Liu, R. Liu, X. Zhao, L. Sun, J. Qu, Adsorptive removal of phosphate by a nanostructured Fe–Al–Mn trimetal oxide adsorbent, Powder Technol., 233 (2013) 146–154.
[37] Z. Gu, B. Deng, J. Yang, Synthesis and evaluation of iron-containing ordered mesoporous carbon (FeOMC) for arsenic adsorption, Microporous Mesoporous Mater., 102 (2007) 265–273.
[38] S.H. Yu, X.L. Dong, H. Gong, H. Jiang, Z.G. Liu, Adsorption kinetic and thermodynamic studies of phosphate onto tantalum hydroxide, Water Environ. Res., 84 (2012) 2115–2122.
[39] C.A. Martinson, K.J. Reddy, Adsorption of arsenic(III) and arsenic(V) by cupric oxide nanoparticles, J. Colloid Interface Sci., 336 (2009) 406–411.

Supplemental information

The detailed calculation for the adsorption section is presented as follow:

S1. Kinetics and thermodynamic studies

Eq. (S1) is used to calculate the adsorption capacity of the adsorbate (i.e., arsenite or phosphate), q_t (mg g^{-1}).

$$q_t = \frac{V \cdot \left(C_i - C_t\right)}{m} \tag{S1}$$

where C_i and C_t are the adsorbate concentrations (mg L^{-1}) at the start and at a specific time t, respectively; m is the adsorbent weight (g); V is the volume of the solutions (L);

The equilibrium adsorption capacity, q_e (mg g^{-1}) is expressed by Eq. (S2).

$$q_e = \frac{V \cdot \left(C_0 - C_e\right)}{m} \tag{S2}$$

where C_e is the dye concentration at equilibrium.

The pseudo-first-order and pseudo-second-order kinetic models were used to interpret the kinetic data. In the non-linear form [S1,S2], the pseudo-first-order kinetic and pseudo-second-order kinetic equations are expressed as Eqs. (S3) and (S4), respectively.

$$q_t = q_e\left(1 - e^{-k_1 \cdot t}\right) \tag{S3}$$

$$q_t = q_e \cdot \frac{q_e \cdot k_2 \cdot t}{1 + q_e \cdot k_2 \cdot t} \tag{S4}$$

where k_1 and k_2 are the rate constant for the pseudo-first-order kinetic the pseudo-second-order kinetic model, respectively.

The non-linear regression method was used with the Solver function in Microsoft Excel to acquire the values of k_1, k_2, and q_e.

S2. Equilibrium adsorption

Using 0.05 g of La_2O_3 in a 100 mL flask of arsenite solution (10 mg L^{-1}) or phosphate solution (50 mg L^{-1}), the temperature influence on phosphate or arsenite adsorption was examined. The adsorption/desorption equilibrium was obtained by magnetically stirring the flasks with seals for 7 h at a given temperature. The equilibrium adsorbate concentration in the filtrate was measured. The following is the distribution coefficient, K_d:

$$K_d = \frac{C_i - C_e}{C_e} \tag{5}$$

where C_i and C_e (mg g^{-1}) are the concentration of adsorbate at the initial and at equilibrium time.

Eq. (S6) expresses the change in standard Gibbs free energy of adsorption ($G°$) [S3].

$$\Delta G° = \Delta H° - T\Delta S° \tag{6}$$

where $\Delta G°$, $\Delta H°$, and $\Delta S°$ are the change of standard Gibbs free energy, enthalpy, and entropy, respectively.

Van't Hoff's equation is used to express $G°$.

$$\Delta G° = -RT\ln\left(K_d\right) \tag{7}$$

where K_d is the distribution coefficient.

By replacing Eq. (S7) to Eq. (S6), once obtained.

$$\ln K_d = -\frac{\Delta H°}{RT} + \frac{\Delta S°}{R} \tag{8}$$

The slope and intercept of the line of plot of $\ln K_d$ vs. $1/T$ give the values of $\Delta H°$ and $\Delta S°$.

The equilibrium data is collected using the Freundlich and Langmuir isotherm models.

Langmuir isotherm model is expressed as Eq. (S9) [S4].

$$q_e = \frac{K_L \cdot q_m \cdot C_e}{1 + K_L \cdot C_e} \tag{9}$$

where q_m is the maximum monolayer capacity amount (mg g^{-1}); K_L is the Langmuir equilibrium constant (L mg^{-1}); q_e (mg g^{-1}) and C_e (mg L^{-1}) is the equilibrium adsorption capacity.

Freundlich isotherm model is represented as Eq. (S10) [S5].

$$q_e = K_F \cdot C_e^{1/n} \tag{10}$$

where K_F is the Freundlich constant; n is the empirical parameter.

Using the Solver function in Microsoft Excel, the model parameters were calculated from the non-linear regression.

References

[S1] R.L. Tseng, F.C. Wu, R.S. Juang, Characteristics and applications of the Lagergren's first-order equation for adsorption kinetics, J. Taiwan Inst. Chem. Eng., 41 (2010) 661–669.
[S2] M.A. Al-Ghouti, M.A.M. Khraisheh, M.N.M. Ahmad, S. Allen, Adsorption behaviour of methylene blue onto Jordanian diatomite: a kinetic study, J. Hazard. Mater., 165 (2009) 589–598.
[S3] R. Menhage-Bena, H. Kazemian, M. Ghazi-Khansari, M. Hosseini, S.J. Shahtaheri, Evaluation of some natural zeolites and their relevant synthetic types as sorbents for removal of arsenic from drinking water, Iran. J. Public Health, 33 (2004) 36–44.
[S4] I. Langmuir, The constitution and fundamental properties of solids and liquids. Part I. Solids, J. Am. Chem. Soc., 38 (1916) 2221–2295.
[S5] "Inside Front Cover (Ed Board)," Spectrochim. Acta, Part A, 135 (2015).